Simultaneous Measurement of Temperature and Strain with Enhanced Accuracy by Using Forward Brillouin Scattering in Highly Nonlinear Fiber

Guijiang Yang, Keyan Zeng, Liang Wang,* Ming Tang, and Deming Liu

National Engineering Laboratory for Next Generation Internet Access System, School of Optics and Electronic Information & Wuhan National Lab for Optoelectronics (WNLO), Huazhong University of Science and Technology, Wuhan 430074, China

**E-mail: hustwl@hust.edu.cn*

Abstract: Simultaneous temperature and strain sensing has been demonstrated for the first time by using forward Brillouin scattering in highly nonlinear fiber. The accuracy is improved by seven times compared with that using backward Brillouin scattering.

1. Introduction

Distributed Brillouin optical fiber sensors have attracted plenty of research interest due to their excellent capability of temperature and strain sensing over long distance [1]. Those sensors are based on backward Brillouin scattering (BBS). However, there is cross-sensitivity of temperature and strain in BBS, which makes simultaneous measurement of temperature and strain difficult [2]. To overcome this, hybrid sensing systems combining BBS with Rayleigh/Raman scattering have been proposed [3]. Using fibers with multi-peak Brillouin gain spectrum (BGS) is also reported to be an effective and simple way of measuring both the temperature and strain [4]. Neverthelss, a microwave source with a frequency range reaching ~10GHz is needed for the measurement since the Brillouin frequency shift (BFS) of BBS is usually around ~10GHz, which makes the setup expensive. Moreover, due to the relatively wide BGS linewidth (tens of MHz), not only multiple frequency scans are needed, but also measurement errors are usually large when extracting the BFS from the BGS.

On the other hand, forward Brillouin scattering (FBS) can be stimulated when the incident light interacts with transverse acoustic waves along the fiber radial direction [5]. The acoustic resonance frequency in FBS is typically in the range of hundreds of MHz to several GHz, and the linewidth of the FBS gain spectrum is several MHz, both of which are much lower than those in BBS. There are some few works using FBS to measure a single temperature or strain [6-8]. But the cross-sensitivity of temperature and strain still exists in FBS. Recently, L. A. SÁNCHEZ et al. have used FBS in a long-period grating to distinguish the temperature and strain [9]. However, the grating requires a change of the fiber structure and is not feasible for distributed sensing. In this paper, we have proposed and demonstrated for the first time the use of FBS in a highly nonlinear fiber (HNLF) to achieve simultaneous measurement of temperature and strain. The proposed method only requires the radio frequency measurement in the range of 1.5 GHz, which can be achieved accurately with less expensive equipment. The narrow linewidth of the FBS gain spectrum together with the large FBS gain in HNLF greatly enhances the sensing accuracy when compared with that of BBS-based sensors.

2. Principle and simulation

The transverse acoustic modes involved in the forward Brillouin scattering inside the fiber are radial acoustic modes $R_{0,m}$ and torsional-radial acoustic modes $TR_{2,m}$. The resonance frequencies of $R_{0,m}$ and $TR_{2,m}$ are related to the longitudinal and shear acoustic velocities in the fiber, respectively, which are linearly dependent on both the temperature and strain [9]. Thus the resonance frequencies (forward Brillouin frequency shift, FBFS) of $R_{0,m}$ and $TR_{2,m}$ have linear temperature and strain dependence but with different responses. Using the FBFS of an unstrained fiber at room temperature as a reference, the relative frequency shifts of $R_{0,m}$ and $TR_{2,m}$ under the change of temperature ΔT and strain $\Delta\varepsilon$ can be expressed as:

$$\frac{\Delta f_R}{f_R} = C_T^R \bullet \Delta T + C_\varepsilon^R \bullet \Delta\varepsilon\,, \quad \frac{\Delta f_{TR}}{f_{TR}} = C_T^{TR} \bullet \Delta T + C_\varepsilon^{TR} \bullet \Delta\varepsilon \tag{1}$$

where $\Delta f_R/f_R$ and $\Delta f_{TR}/f_{TR}$ are the relative frequency shifts of $R_{0,m}$ and $TR_{2,m}$. C_T^R (C_T^{TR}) and C_ε^R (C_ε^{TR}) are the temperature and strain coefficients for $R_{0,m}$ ($TR_{2,m}$). By solving the above two equations, both ΔT and $\Delta\varepsilon$ can be obtained from the measurement of the two FBFSs. The errors for the measured temperature and strain can be theoretically expressed as [10]:

$$S_{\Delta T} = \frac{\sqrt{\left(C_\varepsilon^{TR} \bullet S_R\right)^2 + \left(C_\varepsilon^R \bullet S_{TR}\right)^2}}{\left|C_T^R \bullet C_\varepsilon^{TR} - C_\varepsilon^R \bullet C_T^{TR}\right|}, \quad S_{\Delta\varepsilon} = \frac{\sqrt{\left(C_T^{TR} \bullet S_R\right)^2 + \left(C_T^R \bullet S_{TR}\right)^2}}{\left|C_T^R \bullet C_\varepsilon^{TR} - C_\varepsilon^R \bullet C_T^{TR}\right|} \tag{2}$$

where S_R and S_{TR} represent respectively the standard deviation (SD) of the relative frequency shifts of $R_{0,m}$ and $TR_{2,m}$. Since the resonance peaks in FBS have Lorentzian line shapes, S_R and S_{TR} can be further expressed as [11]:

$$S_R = \frac{S_{\Delta f_R}}{f_R} = \frac{1}{f_R \bullet SNR}\sqrt{\frac{3}{4}\delta \bullet \Delta\nu_B}\ ,\quad S_{TR} = \frac{S_{\Delta f_{TR}}}{f_{TR}} = \frac{1}{f_{TR} \bullet SNR}\sqrt{\frac{3}{4}\delta \bullet \Delta\nu_B} \tag{3}$$

where SNR, δ and $\Delta\nu_B$ represent the signal-to-noise ratio (SNR), frequency step and linewidth of the FBS spectrum, respectively. From Eqs. (2) and (3), we can see that high resonance frequency and large SNR of the FBS spectrum, as well as small linewidth, are desirable to achieve low measurement errors. But the FBS spectrum at high resonance frequency usually has low SNR due to its small gain, especially for the case in the standard single-mode fiber (SSMF) where the FBS gain becomes almost zero at high resonance frequency [12]. Thus it is not easy to obtain low errors using SSMF. Here we analyze the forward scattering efficiency for acoustic modes in HNLF based on the theory in Ref. [5]. The simulated scattering efficiency for $R_{0,m}$ and $TR_{2,m}$ modes in HNLF for the resonance frequency range of 0-1.5GHz is shown in Fig. 1. We can see that in HNLF, even for high resonance frequency beyond 1GHz, $R_{0,m}$ and $TR_{2,m}$ still have relatively high scattering efficiency, giving rise to larger FBS gain over a wider range of resonance frequencies and hence better SNR of the FBS spectrum when compared with SSMF. Therefore, it is feasible to use acoustic modes with high resonance frequency in HNLF to achieve low measurement errors. After considering the tradeoff between the SNR and the resonance frequency, $R_{0,30}$ and $TR_{2,49}$ modes in HNLF are selected for simultaneous temperature and strain measurement. Another pair of $R_{0,6}$ and $TR_{2,7}$ modes are also used for comparison.

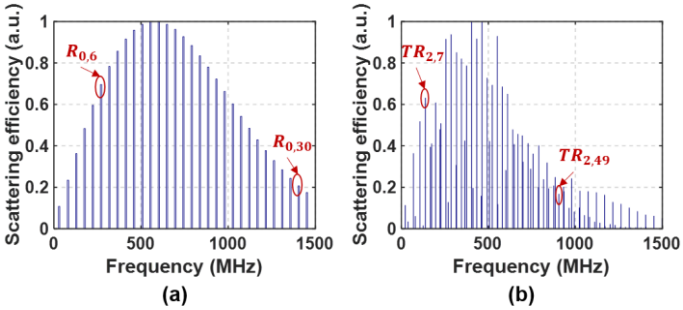

Fig. 1. Simulated scattering efficiency for (a) $R_{0,m}$ and (b) $TR_{2,m}$ modes in HNLF. 127μm cladding diameter and 3.31μm mode field diameter are used in the simulation.

3. Experiment and results

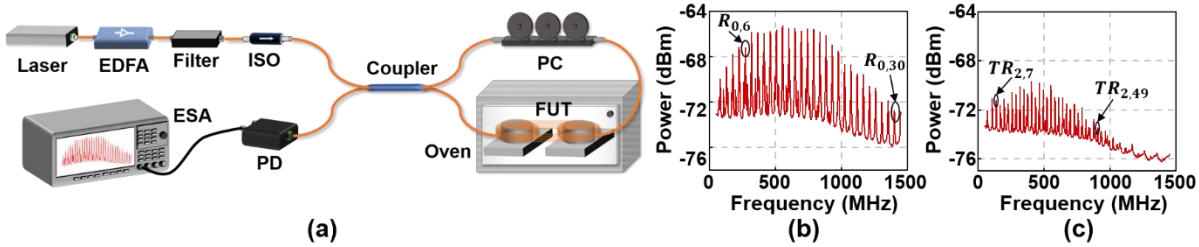

Fig. 2 (a) Experimental setup; (b, c) measured FBS spectra for $R_{0,m}$ and $TR_{2,m}$. EDFA: erbium-doped fiber amplifier; ISO: isolator; PC: polarization controller; FUT: fiber under test; PD: photodetector; ESA: electronic spectrum analyzer.

We adopt a fiber Sagnac loop structure to verify our idea, as shown in Fig. 2(a). The laser output at 1550nm is amplified by an erbium-doped fiber amplifier (EDFA) and is launched into the fiber Sagnac loop. The phase modulation introduced by FBS is converted into amplitude modulation at the output of the loop. The interference signal is detected by a 1.5GHz photodetector (PD) and collected on an electronic spectrum analyzer (ESA). $R_{0,m}$ and $TR_{2,m}$ are distinguished by adjusting the polarization controller (PC). The FUT is a 22m long HNLF coiled on two micro-positioners and is put inside an oven to apply different values of temperature and strain.

Figure 2(b) and (c) depict the measured FBS spectra for $R_{0,m}$ and $TR_{2,m}$ modes when the HNLF is at room temperature without strain. The resonance frequency/linewidth of the FBS spectrum for $R_{0,6}$, $R_{0,30}$, $TR_{2,7}$ and $TR_{2,49}$ are measured to be 271.89MHz/6.21MHz, 1401.85MHz/7.29MHz, 138.3MHz/1.71MHz and 906.44MHz/2.88MHz, respectively. And the SNRs for their FBS spectrum are 18.81dB, 16.42dB, 14.80dB and 13.04dB, respectively. Then we measure the FBS spectrum under two conditions: varying temperature with no strain to obtain C_T^R (C_T^{TR}) and varying strain at room temperature to obtain C_ε^R (C_ε^{TR}). Figure 3(a)-(d) show the measured FBS spectra for $R_{0,30}$ and $TR_{2,49}$, respectively. The relationships between the resonance frequency and temperature/strain are given in Fig. 3(e) and (f). We can see that both the resonance frequencies of $R_{0,30}$ and $TR_{2,49}$

have a linear dependence on the temperature and strain. The results are similar for the case of $R_{0,6}$ and $TR_{2,7}$ modes, as shown in Fig. 3(g) and (h). Based on Fig. 3, the temperature and strain coefficients are calculated to be C_T^R=1.02 × 10^{-4}/°C & C_ε^R =3.3 × 10^{-7}/με for $R_{0,m}$, and C_T^{TR}=7.6 × 10^{-5}/°C & C_ε^{TR}=5.3 × 10^{-7}/με for $TR_{2,m}$, respectively. Using the above parameters in Eqs. (2) and (3), we can derive the theoretical temperature and strain error. For $R_{0,30}$ and $TR_{2,49}$, the theoretical temperature/strain error is 0.18°C/41.87με, while for $R_{0,6}$ and $TR_{2,7}$ it is 0.55°C/136.72με, which is about 3.8 times worse than the former one. Obviously using acoustic modes at high resonance frequency results in low temperature/strain error. As a comparison, we can also estimate the theoretical error of the BBS-based sensor using Eqs. (2) and (3) ($SNR = 20$dB, $\delta = 1MHz$, $\Delta v_B = 65MHz$ in Ref. [4]), which is 7.23°C/296.17με. We can see that the error using FBS is at least seven times lower than that using BBS.

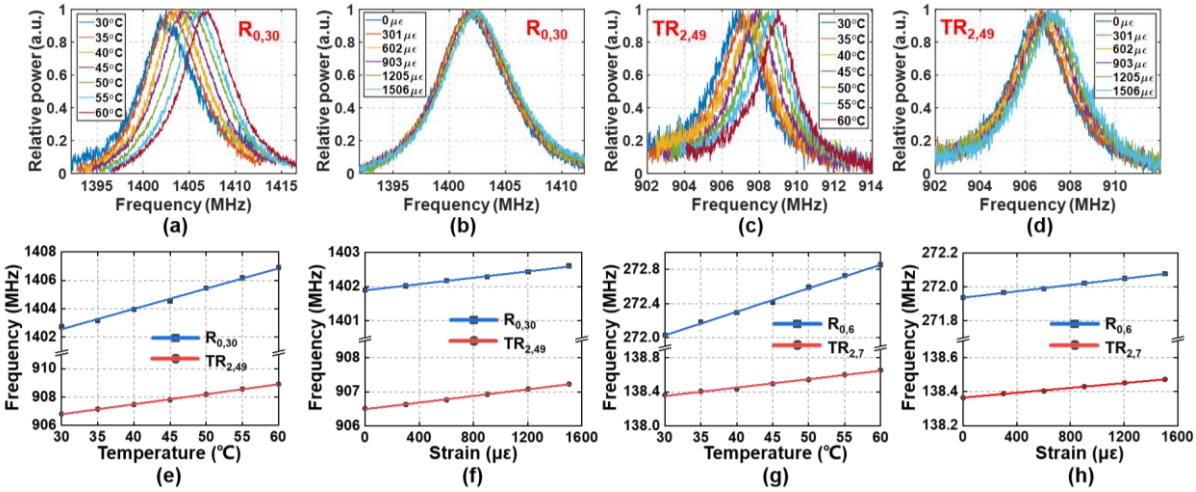

Fig. 3 Measured FBS spectra under different temperature or strain values for (a, b) $R_{0,30}$ and (c, d) $TR_{2,49}$; (e, f) resonance frequency versus temperature/strain for $R_{0,30}$ and $TR_{2,49}$; (g, h) resonance frequency versus temperature/strain for $R_{0,6}$ and $TR_{2,7}$, respectively.

Finally, two different groups of temperature and strain are used for the demonstration of simultaneous temperature and strain measurement. Table 1 shows the experimental temperature and strain error (represented by SD) by using $R_{0,30}$ & $TR_{2,49}$ and $R_{0,6}$ & $TR_{2,7}$, respectively. The SD is obtained by repeating the measurement ten times. The average experimental error using $R_{0,30}$ and $TR_{2,49}$ is 0.15°C/50.94με, which is two times lower than that using $R_{0,6}$ and $TR_{2,7}$. Therefore, using acoustic modes at high resonance frequency in HNLF can enable accurate measurement of both the temperature and strain in a cost-effective way.

Table 1. Experimental temperature and strain error of the proposed method

Temperature/strain	SD by $R_{0,30}$ and $TR_{2,49}$	SD by $R_{0,6}$ and $TR_{2,7}$
30.2°C / 1053.96με	0.16°C / 54.31με	0.44°C / 122.49με
40.6°C / 150.56με	0.14°C /47.57με	0.47°C /136.60με

4. Conclusion

Simultaneous temperature and strain sensing has been demonstrated by using a pair of $R_{0,m}$ and $TR_{2,m}$ modes induced FBS in HNLF. The experimental temperature/strain error by using $R_{0,30}$ and $TR_{2,49}$ modes is two times lower than that by using $R_{0,6}$ and $TR_{2,7}$ modes. Compared with BBS-based sensors, the proposed sensor only requires frequency measurement around 1.5GHz, which is cost-effective without the need of ~10GHz microwave source, and its accuracy is improved by seven times due to the small FBS resonance frequency and linewidth. Moreover, it is feasible for distributed sensing if combined with the technique of time-domain analysis [13].

Acknowledgment

National Natural Science Foundation of China (62005087), Science Foundation of Donghai Laboratory (DH-2022KF01015).

References

[1] F. Bastianini et al., Sensors, **19**(23), 5172 (2019).
[2] C. Hong et al., Sens. Actuators, A **258**, 131–145 (2017).
[3] K. Kishida et al., Photonic Sens., **4**(1), 1–11 (2014).
[4] G. Yang et al., Opt. Exp., **30**(19), 34453-34467 (2022).
[5] R. M. Shelby et al., Phys. Rev. B, **31**(8), 5244 (1985).
[6] Y. Tanaka et al., IEEE Photonics Technol. Lett., **11**(7), 865-867 (1999).
[7] Y. Antman et al., Proc. SPIE, 9634, 96345C (2015).
[8] Hayashi et al., Appl. Phys. Exp., **10**(9), 092501 (2017).
[9] L. A. Sánchez et al., Opt. Exp., **30**(9), 14384-14392 (2022).
[10] J. R. Taylor et al., An Introduction to Error Analysis (University Science Books, 1997).
[11] Marcelo A. Soto et al., Opt. Exp., **21**(25), 31347-31366 (2013).
[12] J. Wang et al., Opt. Exp., **19**(6), 5339-5349 (2011).
[13] C. Pang et al., Optica **7**, 176-184 (2020).